Article

Understanding the Interplay between Self-Assembling Peptides and Solution Ions for Tunable Protein Nanoparticle Formation

Bhuvana Kamath Shanbhag, Chang Liu, Victoria S Haritos, and Lizhong He

ACS Nano, **Just Accepted Manuscript** • DOI: 10.1021/acsnano.8b02381 • Publication Date (Web): 21 Jun 2018

Understanding the Interplay between Self-Assembling Peptides and Solution Ions for Tunable Protein Nanoparticle Formation

Bhuvana K. Shanbhag[†], Chang Liu[†], Victoria S. Haritos[†], Lizhong He[†,]*

†Department of Chemical Engineering, Monash University, Wellington Road, Clayton, VIC 3800, Australia.

KEYWORDS: Peptide self-assembly, protein-protein interaction, non-covalent assembly, metal-ion interaction, pH effect, cross-linking mass spectrometry.

ABSTRACT: Protein based nanomaterials are gaining importance in biomedical and biosensor applications where tunability of the protein particle size is highly desirable. Rationally-designed proteins and peptides offer control over molecular interactions between monomeric protein units to modulate their self-assembly and thus particle formation. Here, using an example enzyme-peptide system produced as a single construct by bacterial expression, we explore how solution conditions affect the formation and size of protein nanoparticles. We found two independent routes to particle formation, one facilitated by charge interactions between protein-peptide and peptide-peptide exemplified by pH change or presence of NO_3^- or NH_4^+, and the second route *via* metal ion coordination (*e.g.* Mg^{2+}) within peptides. We further demonstrate that the two independent factors of pH and Mg^{2+} ions can be combined to regulate nanoparticle size. Charge interactions between protein-peptide monomers play a key role in either promoting or

suppressing protein assembly; the intermolecular contact points within protein-peptide monomers involved in nanoparticle formation were identified by chemical cross-linking mass spectrometry. Importantly, the protein nanoparticles retain their catalytic activities, suggesting that their native structures are unaffected. Once formed, protein nanoparticles remain stable over long periods of storage or with changed solution conditions. Nevertheless, formation of nanoparticles is also reversible – they can be disassembled by desalting the buffer to remove complexing agents (*e.g.* Mg^{2+}). This study defines the factors controlling formation of protein nanoparticles driven by self-assembly peptides and an understanding of complex ion-peptide interactions involved within, offering a convenient approach to tailor protein nanoparticles without changing amino acid sequence.

Controlling self-assembly of proteins and peptides to form nanostructures is becoming an essential means for synthesis of functional biomaterials[1,2] and for biomedical applications.[3,4] Although computational approaches are powerful methods that have successfully guided design of proteins to form nanostructures with high accuracy at atomic levels,[5,6] it still remains a challenge to confer self-assembly properties into proteins by site-directed mutagenesis without compromising their functionality. Instead of directly changing amino acid residues of proteins, a complementary approach is fusing functional proteins with self-assembly peptides to form protein nanofiber scaffolds[7] and protein vesicles.[8] Protein-peptide fusions have been promising candidates for the formation of protein assemblies such as nanoparticles[9] and large-cage structures[10,11] with biocatalytic applications.

Protein nanomaterials of desirable sizes are essential to achieve optimal functions that suit specific applications such as cell imaging,[3] vaccine[12] and drug delivery.[13–15] Particularly,

vaccines based on assembling protein nanoparticles must have appropriate sizes to elicit sufficient immune response to improve potency and breadth of immunity.[12,16] The cellular uptake efficiency of protein nanoparticles, their interactions with cells and final localization have shown strong correlations with the nanoparticle sizes.[13,14] As an emerging delivery vehicle for therapeutic proteins, protein nanoparticle having tunable sizes offers the flexibility to either load functional proteins on the surface of nanoparticles for extracellular delivery or encapsulate them internally within nanoparticles to protect against degradation by proteinases.[15] A convenient method that allows easy control of size of protein nanoparticles is thus highly valuable.

Regardless of different protein engineering approaches, self-assembly of proteins and peptides are influenced by solution conditions such as pH, temperature and the presence of salts. For instance, formation of gels by self-assembly of designed peptides has been controlled by pH,[17] metal ions like calcium,[18] potassium[19] and of spherical protein-polymer micelles triggered by change in temperature.[20] Enzymatic hydrogels have been formed under controlled conditions and mixing ratios of the individual components.[21,22] Despite this progress, it is still difficult to control the assembled structures, in part, due to lack of a fundamental understanding of protein self-assembly into nanomaterials. Current knowledge of protein self-assembly mechanisms are restricted to areas of crystallization, viral particles and amyloid fibrils.[23] In this work, we explore the factors that affect protein nanoparticle formation using our model enzyme-peptide system - bovine carbonic anhydrase (BCA) linked with a $P_{11}4$ peptide (BCA-$P_{11}4$),[9] which can be readily produced from a single DNA construct using the bacterium *E. coli* in high yield. We first examined the effects of pH and ionic strength on formation of protein nanoparticles, and suggested interactive forces for their formation. The intermolecular protein-peptide contacts within nanoparticles were identified by cross-linking followed by mass spectrometry. After

examining the effects of salts on nanoparticle formation, we studied another assembly mechanism where magnesium ions were used as the initiator. We then investigated how nanoparticle formation could be controlled by a combination of different modulators. After examining the functionalities and stabilities of protein nanoparticles, we tested whether the presence of other biomolecules affected assembly of protein nanoparticles, aiming to give a comprehensive description of formation of this different type of nanoparticle.

RESULTS AND DISCUSSION

Control of nanoparticle formation by pH and ionic strength. Firstly, the effect of varying pH on BCA-P_{11}4 at 0.5 mg/mL was examined in low ionic strength buffer of 10 mM Tris-HCl. As shown in Figure 1a, when pH was reduced to 6.8, no formation of BCA-P_{11}4 nanoparticles was observed. The lack of self-assembly prompted us to increase the concentration of the buffer to 50 mM Tris-HCl and retest the effect of pH. As shown in Figure 1b, nanoparticles with an average diameter of 100 nm were formed at pH 6.8 and these gradually increased in size with further reduction in pH. This result demonstrates that self-assembly cannot be achieved solely through pH reduction and requires sufficient amount of Tris to allow adjacent BCA-P_{11}4 monomers to interact and self-assemble into nanoparticles.

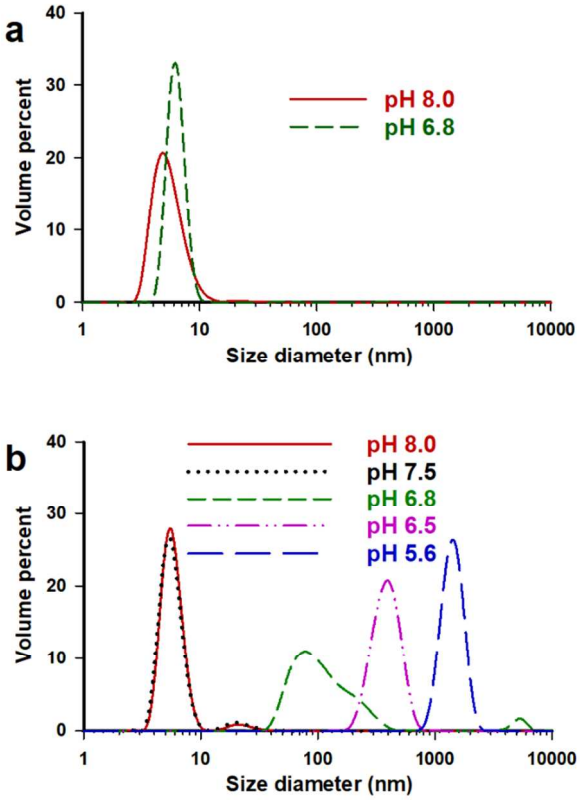

Figure 1. Influence of pH and buffer concentration on BCA-P_{11}4 particle size formation at a BCA-P_{11}4 concentration of 0.5 mg/mL. (a) Low buffer concentration: 10 mM Tris-HCl (b) increased buffer concentration: 50 mM Tris-HCl.

Interactive forces for nanoparticle formation. Based on the observed effects of pH, we propose two interactive forces that influence BCA-P_{11}4 self-assembly: firstly, there is the interaction between peptide-peptide monomers ($F_{pep\text{-}pep}$) in anti-parallel orientation[24] that is a combination of the attractive and repulsive forces as shown in Figure 2a, where attractive forces exist between oppositely positioned arginine and glutamic acid residues and the π-π interaction of aromatic residues while glutamic acid residues at the 5th and 7th peptide position impart

repulsive forces. Secondly, there is a pH-dependent interaction between protein and peptide monomers, $F_{pro\text{-}pep}$ (Figure 2b).

Decreasing pH from 8 to 6.8 results in an insignificant change in charge of $P_{11}4$ from -2.5 to -2 but the charge of BCA changes from -3.4 to a positive +0.7 (Table S1). It is thus expected that lowering pH has no significant effect on peptide-peptide interaction $F_{pep\text{-}pep}$ but prompts a positive intermolecular protein-peptide interaction $F_{pro\text{-}pep}$ that favors assembly (Figure 2b). However, the positive $F_{pro\text{-}pep}$ alone is not sufficient to form nanoparticles at pH 6.8 as we have tested using 10 mM Tris. It requires an enhancement of peptide-peptide interaction $F_{pep\text{-}pep}$ by increase in Tris concentration from 10 to 50 mM. The three forces that collectively determine $F_{pep\text{-}pep}$ (Figure 2a) are influenced by the concentration of Tris. The repulsive forces between negative glutamic acid residues are expected to be reduced at increased buffer concentration as previous research has reported self-assembly of pure $P_{11}4$ peptide regulated by ionic strength to form hydrogels near neutral pH.[25]

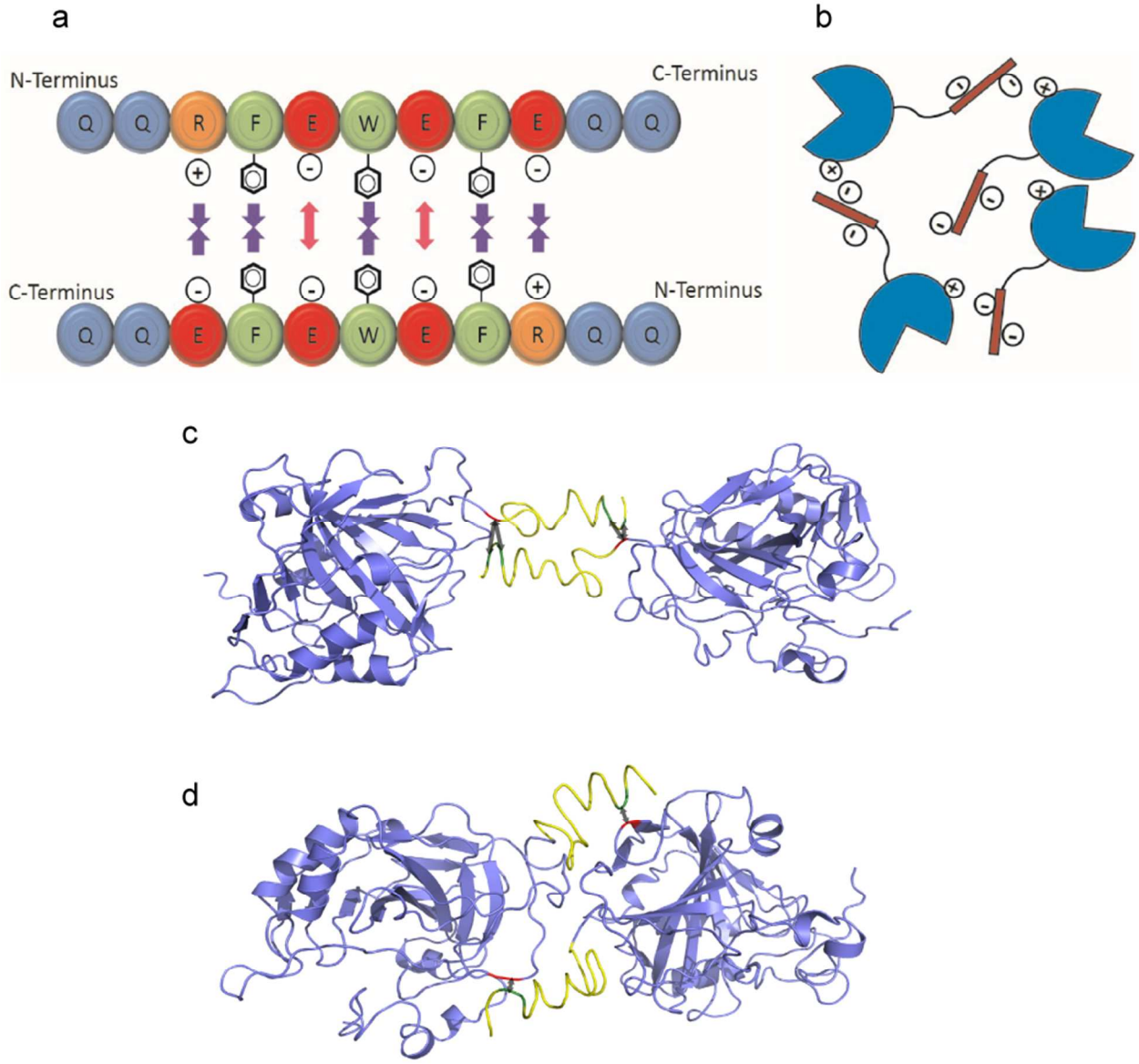

Figure 2. Forces affecting BCA-$P_{11}4$ nanoparticle formation and intermolecular protein-peptide contacts. (a) Illustration of the peptide-peptide force, $F_{pep\text{-}pep}$, between two $P_{11}4$ peptide monomers arranged in an anti-parallel formation at neutral pH, depicting uncharged residues in blue, positively charged residue in orange, aromatic residues in green and negatively charged residues in red. Attractive forces are represented by purple arrows and repulsive forces by pink arrows in the inter-peptide region. (b) Representation of the attractive electrostatic interactions,

$F_{pro\text{-}pep}$, between surface charges of protein-peptide monomers at pH <7, where protein (blue pie-shape) bears one positive charge and the peptide (brown cylinder) bears two negative charges. (c) As seen in the color-coded protein-peptide cartoon, two BCA-$P_{11}4$ monomers interact with each other through peptide-peptide interaction. BCA (marine), linker and $P_{11}4$ (yellow), lysine residues (red), glutamic acid residues (green). Gray double-headed arrows indicate chemical cross-linking. (d) Two BCA-$P_{11}4$ monomers interact with each other through protein-peptide interaction. Same color code as (c).

Further reduction of pH from 6.8 to 6.5 and 5.6, increases particle size due to the larger difference in charge of peptide (-1.8) and protein (+8.5) regions (Table S1) that would drive self-assembly *via* enhanced $F_{pro\text{-}pep}$ interaction. To a lesser extent, lowering of pH causes a loss of negative charge from the acidic group of the glutamic acid residues, [26] which reduces the repulsion between the two peptides and subsequently increases the $F_{pep\text{-}pep}$ forces to be attractive. Essentially, a combination of the two forces $F_{pep\text{-}pep}$ and $F_{pro\text{-}pep}$ are regulated by pH and buffer concentration, controlling the formation of nanoparticles.

Intermolecular protein-peptide contacts. Having proposed possible forces, $F_{pep\text{-}pep}$ and $F_{pro\text{-}pep}$, we further investigated the intermolecular contact points between BCA-$P_{11}4$ monomers within protein nanoparticles. To achieve this, cross-linking of protein nanoparticles was undertaken and key residues identified by mass spectrometry. Two different coupling agents (Figure S3a), bissulfosuccinimidyl suberate (BS3) and 1-ethyl-3-(3-dimethylaminopropyl)-carbodiimide - N-hydroxysulfosuccinimide) (EDC-sNHS), were used to selectively target different amino acid residues. While BS3 targets cross-linking between two lysine residues (Figure S3b), EDC-sNHS targets cross-linking between glutamic acid/aspartic acid and lysine (Figure S3c). Comparing cross-linking results of these two reagents can thus give

complementary information on intermolecular contact points. Interestingly, the EDC-sNHS coupling reaction resulted in a higher molecular weight protein band (~60 kDa), approximately twice the size of the BCA-P_{11}4 monomer by SDS-PAGE (Figure S4). In contrast, the coupling reaction of BS3 showed no cross-linking of two BCA-P_{11}4 monomers by SDS-PAGE (Figure S4). The results thus suggest there are no close interactions of lysine residues while lysine and glutamic acid residues are in close contact in assembled BCA-P_{11}4 particles. The 60 kDa band from EDC-sNHS coupling was further analyzed by ESI-MS/MS, and peptide mapping data (Table S2) identified 4 key intermolecular cross-linked locations (K261-E280, K261-E278, E278-K81, K252-E278). Based on these data, we are able to highlight points of interaction between BCA-P_{11}4 monomers within assembled nanoparticles, including sites of peptide-peptide (Figure 2c) and protein-peptide (Figure 2d) interactions.

Effect of salt addition on nanoparticle formation. The required increase of Tris concentration from 10 mM and 50 mM for nanoparticle formation prompted us to investigate whether this effect is simply attributed to the change of ionic strength or more specific contribution of buffering ions. It has been reported in literature that hydroxyl groups of Tris can specifically interact with amino acids such as Asp, Glu and Ala[27] and strongly interact with peptide backbone.[28] Our first test was carried out by adding 50 mM NaCl or NH_4Cl to 10 mM Tris-HCl at pH 8.0 followed by pH adjustment to 6.8. Surprisingly, the two salts had opposite effects. With the addition of NaCl, nanoparticle formation was not observed (Figure 3a) while the addition of NH_4Cl promoted nanoparticle formation with two size peaks (88 and 260 nm) at pH 6.8 (Figure 3b). This result suggests that specific ions rather than a simple increase of ionic strength is required for pH triggered nanoparticle formation.

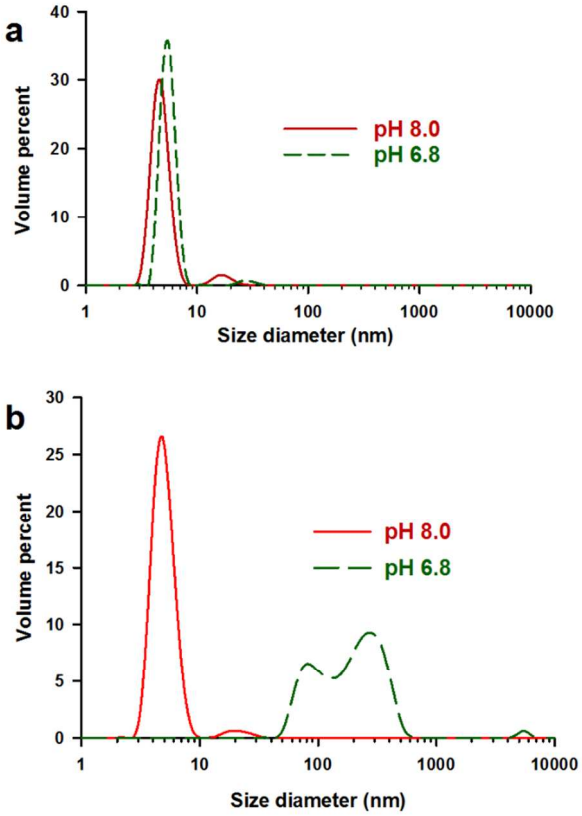

Figure 3. Influence of salt addition on BCA-$P_{11}4$ particle formation at a protein concentration 0.5 mg/mL in 10 mM Tris-HCl (a) 50 mM NaCl; (b) 50 mM NH_4Cl.

To explore how salts can influence pH-triggered BCA-$P_{11}4$ self-assembly, we investigated the effect of cations Na^+ and NH_4^+ as chloride salts at concentrations higher than those previously described together with the effect of addition of a range of anions known to influence protein stability or solubility[29] added as sodium salts: SO_4^{2-}, Cl^-, NO_3^-. Formation of nanoparticles was studied in 10 mM Tris-HCl buffer and at two pH values, pH 6.5 and 8.0 (Table 1). No self-assembly was observed at pH 8.0 in the presence or absence of all salts because at this pH, BCA-$P_{11}4$ bears a net charge of -5.4 causing repulsive forces to dominate (Table S1). However, at pH

6.5 nanoparticles were produced in the presence of two salts, NH_4Cl and $NaNO_3$. By comparing the combinations of different anions and cations (table 1), it appears that none of SO_4^{2-}, Cl^-, and Na^+ contributes to formation of protein nanoparticles, but both NH_4^+ and NO_3^- ions have significant contributions.

Ammonium chloride promoted self-assembly of BCA-P_{11}4 at concentrations up to 100 mM. It is well-known that the NH_4^+ ion can have a strong interaction with protein and peptide surfaces, particularly through its ability to form cation-π interactions[30] with aromatic amino acids. Since the self-assembly peptide is rich in aromatic amino acids (two phenylalanine and one tryptophan amino acids), it is expected that the presence of NH_4^+ may enhance the $F_{pep\text{-}pep}$ forces by forming multiple cation-π interactions. This increased $F_{pep\text{-}pep}$ force by NH_4^+, together with the enhanced $F_{pro\text{-}pep}$ force introduced by the decrease of pH, promotes formation of protein nanoparticles.

The distinctive attributes of NO_3^- compared with Cl^- and SO_4^{2-} deserves further discussion. While all three ions can take part in anion-π interactions,[31] NO_3^- ion is distinguished as it adopts a trigonal planar configuration and is highly polarized with a formal positive charge on the nitrogen and the 3 oxygens sharing the two negative charges. A NMR study by Watt *et al* [32] has shown that NO_3^- has strongest affinity for the tripodal urea receptor in the order of $NO_3^- > Cl^- > Br^- > I^-$. Directly related to the protein used in the current research, molecular dynamic simulation study has indeed demonstrated that NO_3^- is closely associated with the BCA surface residues; the shortest association peaks were within 2 Å of the surface whereas Cl^- ion had a more diffuse association with the protein surface.[33] NO_3^- ion thus in closer proximity can facilitate the formation of protein nanoparticles upon decrease of pH.

Table 1. Influence of added salts and pH on self-assembly of BCA-P_{11}4*

Salt	Concentration (mM)	pH 8.0	pH 6.5
NaCl	50	-	-
	100	-	-
	200	-	-
NH_4Cl	50	-	+
	100	-	++
	200	-	-
Na_2SO_4	50	-	-
	100	-	-
	200	-	-
$NaNO_3$	50	-	+
	100	-	-
	200	-	-

* Particles formed in 10 mM Tris-HCl buffer with added salts and size measured by dynamic light scattering indicated by "+" for particle size < 500nm, "++" for particle size > 500nm and "-" no nanoparticle

It should be noted, irrespective of the salt used, no self-assembly was observed with addition of the salts at 200 mM at either pH 8.0 or pH 6.5. We attribute this phenomenon in the assembly

process to the effect of charge screening by the additional ions which weakens attractive charge interactions between protein and peptide $F_{pro\text{-}pep}$, and also decreases attractive peptide-peptide force $F_{pep\text{-}pep}$ as previously reported.[26] In the following sections, the effect of ionic strength on stability of formed nanoparticle is further discussed. Based on the interactions described in this study, there is a large potential to investigate the specific effect of ion-type[29] to manipulate self-assembly of protein-peptide. Especially for proteins carrying distinct polarities, it may be vital to understand preferential interaction parameters[34] that govern protein-protein interactions, for example, quantification of the contribution of anion-π interactions.[31]

An alternative mechanism of nanoparticle formation by magnesium ions. Next, the effects of divalent cations on the BCA-P_{11}4 nanoparticle were examined as these are well known to form co-ordination bonds between individual monomeric protein units and promote self-assembly independent of pH change. For example, zinc ions promote the peptide AM1 to form strong films at neutral pH[35] and similarly calcium cross-links beta roll peptides which form hydrogels.[36] The effects of the chloride salts of Ca^{2+} and Mg^{2+} on BCA-P_{11}4 self-assembly were evaluated in parallel with wild-type BCA in order to understand their binding to protein surfaces. Ca^{2+} promoted formation of BCA-P_{11}4 nanoparticles at pH 8.0 but also with wild-type BCA which lacks the self-assembling peptide (Figure S6), suggesting a non-specific effect of this cation between residues at the protein surface. On the contrary 25 mM Mg^{2+} promoted BCA-P_{11}4 self-assembly at pH 8.0 while showing no influence on protein size with wild-type BCA alone under similar conditions (Figure 4a), suggesting a specific Mg^{2+} interaction involving the peptide region of BCA-P_{11}4. In terms of controlled assembly of nanoparticles, Mg^{2+} is the preferred

cation because its interaction for nanoparticle formation is primarily with the peptide region and its interaction with protein is insignificant as demonstrated with the wild-type BCA.

The nanoparticle-forming effect observed with $MgCl_2$ on BCA-$P_{11}4$ also presents a potential alternative approach to generate nanoparticles using certain metal ions without adjusting pH, once conditions for controlling the assembly of particles is better understood. We examined the effect of different $MgCl_2$ concentrations on BCA-$P_{11}4$ self-assembly by dynamic light scattering. Nanoparticles were formed in 10 mM Tris-HCl pH 8.0 buffer at $MgCl_2$ concentration as low as 5 mM while larger nanoparticles were favored at 25 mM $MgCl_2$ (Figure 4b). Transmission electron microscopy imaging confirmed the presence of BCA-$P_{11}4$ nanoparticles with diameter in the range of 100-200 nm formed at 5 mM $MgCl_2$ (Figure 4c). At concentrations above 25 mM $MgCl_2$, a reduction in particle size was observed with no self-assembly beyond 75 mM. The dependence of BCA-$P_{11}4$ self-assembly on $MgCl_2$ concentration can be explained by the change of Debye length, κ^{-1}, of Mg^{2+} ion. In the concentration range of 5-25 mM, the Debye length of Mg^{2+} ions was estimated to range from 1.44 to 0.64 nm using the formula κ^{-1} (nm) = $0.176/[MgCl_2]^{1/2}$.[37] These relatively large Debye lengths facilitate simultaneous ionic interactions of one Mg^{2+} ion with two nearby peptides. Within this concentration region, the increase of Mg^{2+} concentration improves the chance of Mg^{2+} ions interacting with BCA-$P_{11}4$ peptides, leading to larger protein particles. However, with a further increase in $MgCl_2$ concentration, the Debye length is significantly reduced. For example, it has a value of 0.37 nm at $MgCl_2$ concentration of 75 mM, possibly preventing one Mg^{2+} ion interacting with two peptides at the same time. Similar effects of Mg^{2+} concentration have been reported for the multi-layer self-assembly of amyloid-like peptides at mica/water interface.[38]

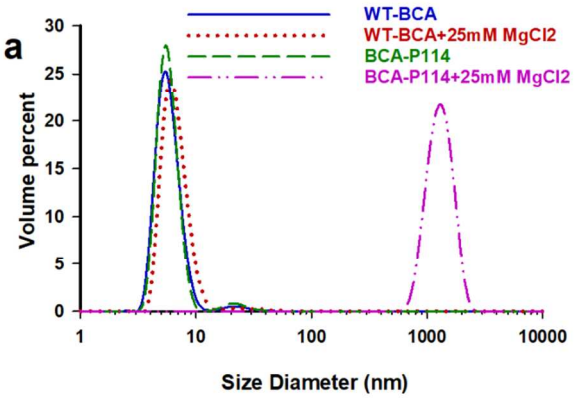
a
WT-BCA
WT-BCA+25mM MgCl2
BCA-P114
BCA-P114+25mM MgCl2
Volume percent
Size Diameter (nm)

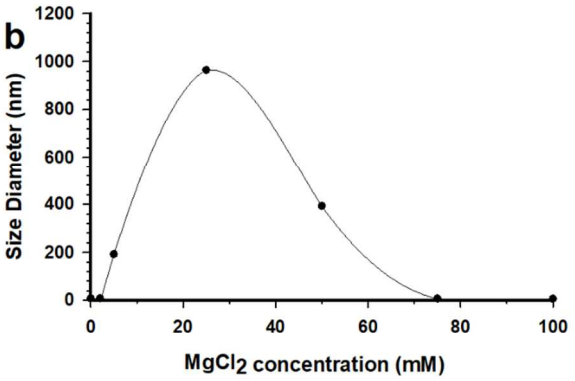
b
Size Diameter (nm)
MgCl2 concentration (mM)

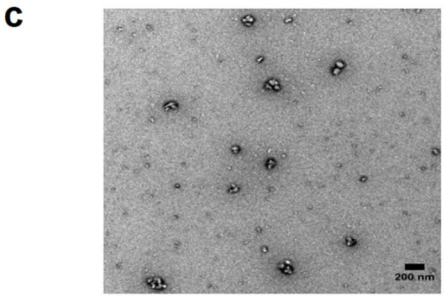
c
200 nm

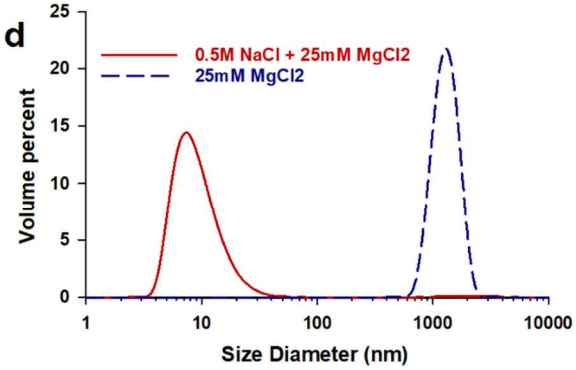
d
0.5M NaCl + 25mM MgCl2
25mM MgCl2
Volume percent
Size Diameter (nm)

Figure 4. BCA-$P_{11}4$ nanoparticle formation facilitated by $MgCl_2$ in 10mM Tris-HCl pH 8.0 buffer at a protein concentration of 0.5 mg/mL(a) Effect of 25 mM $MgCl_2$ on wild-type BCA and BCA-$P_{11}4$; (b) Effect of $MgCl_2$ concentration on BCA-$P_{11}4$ nanoparticle size; (c) TEM image of BCA-$P_{11}4$ nanoparticles formed in 5 mM $MgCl_2$; (d) Size distribution by dynamic light scattering illustrating that the presence of 0.5 M NaCl in the assembling buffer inhibits Mg^{2+}-facilitated BCA-$P_{11}4$ self-assembly.

Here, we propose a molecular mechanism for the controllable formation of BCA-$P_{11}4$ nanoparticles with Mg^{2+}. In solution but in the absence of proteins, Mg^{2+} ions exist in a stable coordination complex with 6 oxygen atoms contributed by water.[39] However, in the presence of protein, Mg^{2+} has a stronger interaction with oxygen atoms from carboxyl and hydroxyl groups in the side chain residues of amino acids.[40] Figure 5a illustrates the interaction of Mg^{2+} with the carboxyl oxygen of glutamic acid residues in $P_{11}4$ monomers. Since the preferred coordination number for Mg^{2+} is 6, it is possible that this state may be satisfied by 2 or more oxygen atoms of glutamic acid residues from BCA-$P_{11}4$ molecules and the rest with nearby water molecules. The preference of oxygen atoms of glutamic acid over those of water molecules depends directly on the proximity of Mg^{2+} to these molecules, or indirectly, to the size of the Debye sphere whose radius equals the Debye length of Mg^{2+}. In high ionic strength solutions such as 75 mM $MgCl_2$, the size of the Debye sphere of Mg^{2+} is expected to be smaller as Debye length decreases proportionally to square root of the ionic strength (Figure 5b). In essence, one Mg^{2+} ion can no longer simultaneously bind four separate glutamic acid residues of two individual $P_{11}4$ monomers, preventing self-assembly. Our hypothesis of ionic strength effect was tested by measuring particle size in the absence and presence of 0.5 M NaCl in the assembling buffer (Figure 4d) having concentration of 25 mM $MgCl_2$. Indeed, the presence of 0.5 M NaCl in the

assembling buffer prevented nanoparticle self-assembly, confirming our hypothesis. We thus conclude that Mg^{2+} promotes self-assembly through ionic interactions with $P_{11}4$ peptide in BCA-$P_{11}4$ and the size of particle can be collectively controlled by Mg^{2+} concentration and ionic strength of solution.

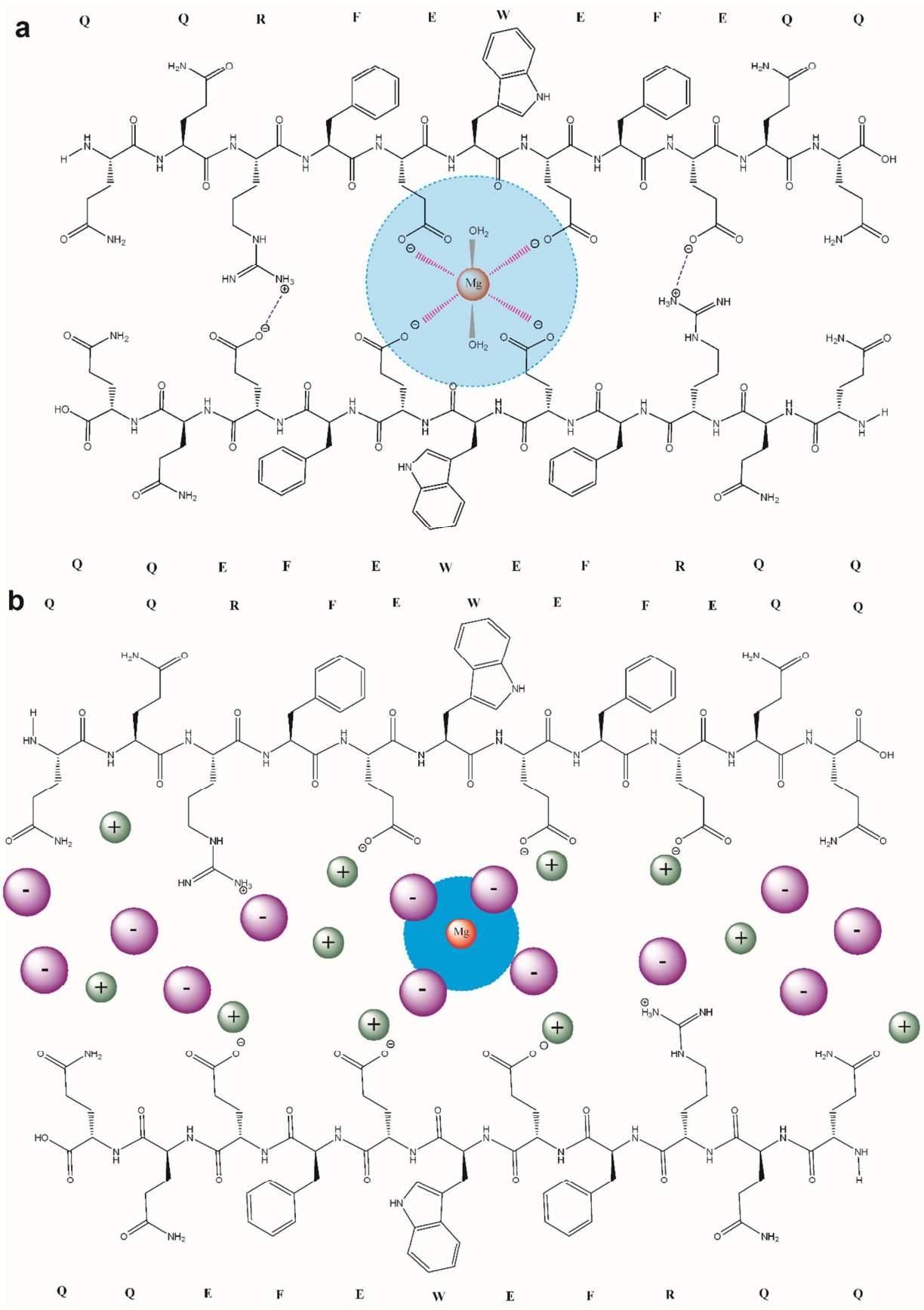
a
Q Q R F E W E F E Q Q
Mg
Q Q E F E W E F R Q Q
b
Q Q R F E W E F E Q Q
Mg
Q Q E F E W E F R Q Q

Figure 5. Proposed mechanism of BCA-P_{11}4 self-assembly in the presence of Mg^{2+} (a) Under low ionic strength, Mg^{2+} with a large Debye sphere (blue filled circle) coordinated to four glutamic acid (E) residues (pink dashed arrow bonds) and two water molecules (gray filled arrow bonds). Self-assembly is further stabilized by electrostatic interaction (blue dashed line) between arginine (R) and glutamic acid (E) residues of adjacent strands. (b) Under high ionic strength, Mg^{2+} has a smaller Debye sphere (blue filled circle), preventing simultaneous interaction of Mg^{2+} with four glutamic acid (E) residues, and BCA-P_{11}4 molecules have weaker assembly ability or do not assemble at all. This schematic model is not to scale.

Control of nanoparticle formation by combination of different modulators. Having established two independent mechanisms to form protein nanoparticles, alteration of pH buffered with specific ions and addition of Mg^{2+}, we further explored the potential for combination of these two conditions when altered simultaneously and any subsequent impact on particle size. As noted in the previous section, addition of Mg^{2+} does not require decrease of pH to form protein nanoparticles, but it requires a certain level of Mg^{2+} concentration (*e.g.* nanoparticles are formed at 5 mM $MgCl_2$, but not at 2 mM $MgCl_2$, figure 4b). Is it possible to form nanoparticles at lower Mg^{2+} concentrations? We first tested whether a combination of 2 mM $MgCl_2$ and decrease of pH from 8.0 to 6.8 can prompt the formation of nanoparticles using two-level factorial design (Table S3). Indeed, nanoparticles were formed with an average size of 350 nm (Table S4) under this changed condition, thus demonstrating that these two factors may be combined to modulate self-assembly under modified solution conditions.

Inspired by this result, we examined the combination of pH change and Mg^{2+} under broader experimental conditions, taking into account effects of temperature and BCA-P_{11}4 concentration (see table S4). The results show that $MgCl_2$ concentration and pH had significant effects on self-assembly. Within the tested range of pH (6.8-8) and $MgCl_2$ concentration (2-20 mM), increase in $MgCl_2$ concentration enlarges nanoparticle size while a lower pH favors nanoparticle formation. In comparison to significant effects of pH and $MgCl_2$ concentration, the protein concentration and temperature have smaller effect on nanoparticle sizes. Based on analysis using factorial design (supporting information), we plot nanoparticle size as a function of pH and $MgCl_2$ concentration (Figure 6a). The 3-D contour plot shows that BCA-P_{11}4 starts from a monomeric form with native size (blue) at pH 8.0 and 2 mM $MgCl_2$, progresses to small particle sizes (green) and reaches to largest particle sizes (orange) at pH 6.8 and 20 mM $MgCl_2$.

Using an empirical equation (Eq S1 in supporting information) resulted from factorial design, we predicted that BCA-P_{11}4 particle with sizes of 253 and 633 nm would be formed under the following conditions – (1) 0.5 mg/mL BCA-P_{11}4, pH 7.5, 6 mM $MgCl_2$, and (2) 1.0 mg/mL BCA-P_{11}4, pH 7.0, 8 mM $MgCl_2$, respectively. Experimental results confirmed the predicted sizes whereby peak centers for conditions 1 and 2 measured by dynamic light scattering were 201 and 669 nm (Figure 6b), respectively. Thus, the particle size of BCA-P_{11}4 can be controlled in a predictable fashion and based on a combination of the two solution conditions.

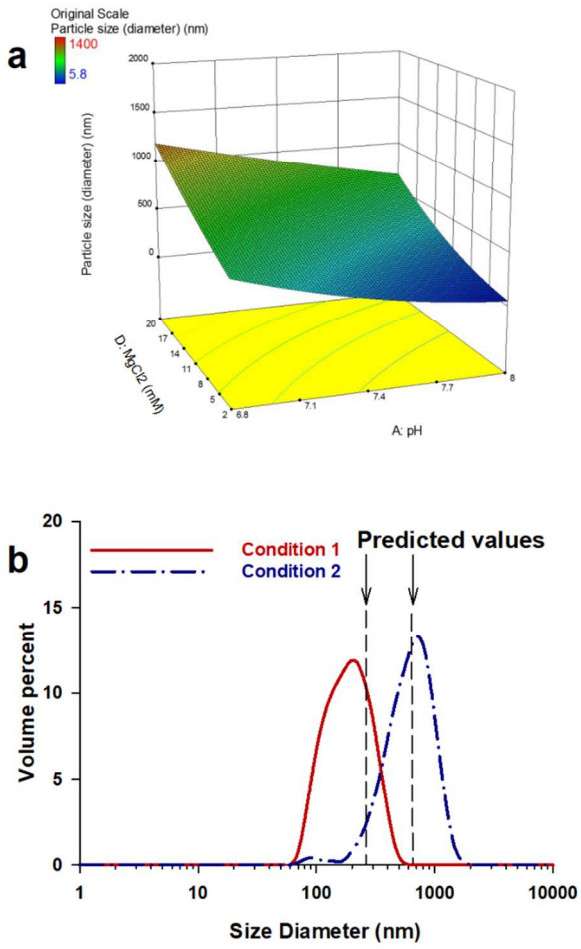

Figure 6. BCA-$P_{11}4$ nanoparticle formation by combination of $MgCl_2$ concentration and pH (a) Particle size as function of $MgCl_2$ concentration and pH; (b) Predicted and actual particle size. Condition 1: 0.5 mg/mL BCA-$P_{11}4$, pH 7.5, 6 mM $MgCl_2$. Condition 2: 1.0 mg/mL BCA-$P_{11}4$, pH 7.0, 8 mM $MgCl_2$

These interesting results lead us to further consider the interplay between BCA-$P_{11}4$ molecules and solution conditions, pH and Mg^{2+}. As discussed previously, Mg^{2+} ions interact with $P_{11}4$ peptides through co-ordination bonds with glutamic acid residues (Figure 5), increasing the peptide-peptide force, $F_{pep\text{-}pep}$. At 2 mM $MgCl_2$ concentration, the Mg^{2+}-induced $F_{pep\text{-}pep}$ force alone is not sufficient to form protein nanoparticles. However, decrease of pH from 8.0 to 6.8 is

expected to increase protein-peptide force, $F_{pro\text{-}pep}$ while it doesn't significantly change $F_{pep\text{-}pep}$. These two forces combined are sufficient to trigger formation of protein nanoparticles at pH 6.8 and 2 mM $MgCl_2$. Furthermore, the combined strength of two forces can be regulated by fine-tuning solution conditions (Figure 6a and Table S4), making it possible to control the particle size in a predictable fashion.

Protein nanoparticles maintain full functionality. Esterase activities of BCA were determined for the various protein nanoparticles formed with different sizes under a broad range of conditions (Table S4). Although there are variations of activities for particles with different sizes, BCA-P_{11}4 particles retain at least 80% activity relative to monomeric protein as shown in Figure 7. Average activities of the protein particles of various sizes were up to 108% of the relative activity of individual protein–peptide units. Note that the link of P_{11}4 peptide to the protein through genetic engineering causes a very minor reduction in enzyme activity (Table S7). These results together demonstrate that the P_{11}4 peptide allows proper orientation and access to active sites of individual enzyme molecules, and the protein thereby retains its complete functionality after the assembly process.

Although nanoparticle formation is expected to introduce mass transfer resistance, quantitative calculation using time constant analysis has shown that this resistance is negligible in comparison to the relatively slow reaction kinetics of the BCA-catalyzed esterase activity. The half-life time of the substrate, $t_{1/2,}$ is at least 4 magnitudes larger than the intraparticle diffusion time constant, t_{diff} (Table S7). We therefore do not observe a decrease in enzyme activity upon formation of the BCA nanoparticle. However, it should be kept in mind that for a fast enzyme

reaction, for example, a reaction with a half-life time of sub-second, the mass transfer resistance within protein nanoparticle may become significant.

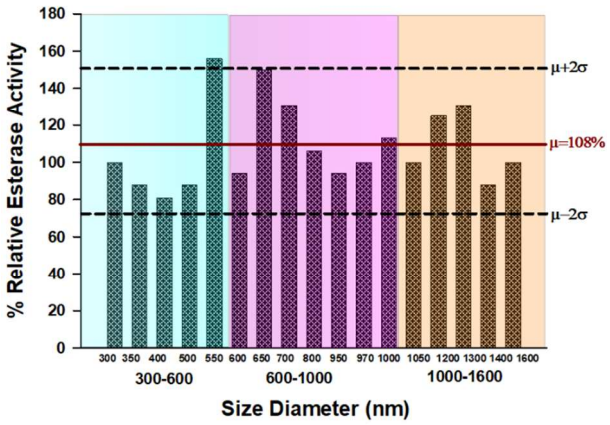

Figure 7. Esterase activity of BCA-P_{11}4 nanoparticles of various sizes measured as a percentage of the monomeric BCA-P_{11}4 fusion protein. Colored areas on the graph indicate various particle sizes Blue: 300-600 nm; Pink: 600-1000 nm; Yellow: 1000-1600 nm. Average activity of all the sizes is shown in brown bold line along with standard deviations (black dashed lines).

Nanoparticles are stable to a change in conditions. Although solution conditions including pH and Mg^{2+} have significant effects on formation of protein nanoparticles, the formed nanoparticles are very stable. For example, while 0.5 M NaCl prevents the formation of nanoparticles (Figure 4d), post-addition of 0.5 M NaCl does not disrupt the protein nanoparticles formed in the presence of 25 mM Mg^{2+} (data not shown). As explained previously, Mg^{2+} has a smaller Debye sphere at a higher ionic strength, preventing it from simultaneously interacting with four separate glutamic acid residues of two individual P_{11}4 peptides when each BCA-P_{11}4 molecule exists as a free monomer in solution. However, once protein nanoparticles are formed, the four glutamic acid residues are in close proximity, and their distance is still smaller than the

Debye length of Mg^{2+} even at increased ionic strength. They can thus retain their existing interactions with Mg^{2+} when 0.5 M NaCl is added post formation of nanoparticles. Effectively, a high ionic strength creates an energy barrier for formation of nanoparticles, but it does not destabilize already formed nanoparticles. That is, protein particles maintain their nanoparticle structure over a broad range of conditions although their successful formation requires a defined solution condition, as demonstrated by the activity measurements presented in Figure 7.

Nanoparticles are stable over storage. We have also tested stability of protein nanoparticles over storage. BCA-P_{11}4 nanoparticles were formed at pH 6.5 in 50 mM Tris-HCl buffer and then stored at 4°C for 1 month. The protein nanoparticles show similar size distribution before and after storage (Figure S9), suggesting that protein nanoparticles are stable over a long period under the storage conditions.

Disassembly of protein nanoparticles. After demonstrating stability of protein nanoparticles over time, we further investigated whether protein nanoparticles can be disassembled in a controllable manner. Formation of BCA-P_{11}4 protein nanoparticles was first initiated by the addition of 5 mM $MgCl_2$. We then fully removed $MgCl_2$ by loading nanoparticle solution onto a desalting column (Figure S10a). The removal of $MgCl_2$ led to disassembly of protein nanoparticles into the monomeric form (Figure S10b). The data shows that the protein nanoparticles can be disassembled in a controllable manner.

Nanoparticle formation in the presence of a second biomolecule. In order to test whether presence of free proteins having surface charges would interfere with BCA-P_{11}4 nanoparticle assembly, we have carried out self-assembly of BCA-P_{11}4 in the presence of wild type BCA

(WT-BCA). Under nanoparticle assembly conditions (10 mM Tris-HCl, pH 8.0, 20 mM $MgCl_2$), WT-BCA has a negative charge of -3.4 but it does not prevent the formation of BCA-P_{11}4 protein nanoparticles (Figure S11). We then tested whether the presence of a positively charged protein, tyrosinase (pI 9.15), affected nanoparticle assembly of BCA-P_{11}4. When $MgCl_2$ was used to initiate self-assembly, BCA-P_{11}4 formed nanoparticles both at pH 8.0 and at a lower pH of 7.2 (Figure S12a). Separately, we also used pH as a sole trigger to form BCA-P_{11}4 nanoparticles in the presence of tyrosinase. It was observed that BCA-P_{11}4 formed nanoparticles when the pH was reduced from 8.0 to 6.4 (Figure S12b). These results show that the presence of either negatively or positively charged biomolecules does not affect the formation of BCA-P_{11}4 nanoparticles when either $MgCl_2$ or pH is used as initiator.

Nanoparticle formation with a different protein. To test whether peptide-mediated protein assembly can be applied to other proteins, we constructed another protein-peptide system, glutathione S-transferase- P_{11}4 (GST-P_{11}4, see full sequence in Supporting Information). After successful expression in *E. coli,* GST-P_{11}4 was purified by immobilized metal-ion affinity chromatography (IMAC). Protein nanoparticle formation with GST-P_{11}4 was investigated using reduced pH or Mg^{2+} ion addition as per BCA-P_{11}4. Nanoparticle formation was successfully initiated with GST-P_{11}4 both *via* reduction of pH from 8.0 to 7.1 as shown in Figure 8a or by the addition of 5 mM $MgCl_2$ (Figure 8b and 8c). These results confirm that the self-assembly of GST-P_{11}4 system is influenced by the same factors of pH, ionic strength and Mg^{2+} ions as BCA-P_{11}4. The further exemplification with GST-P_{11}4 suggests that peptide-mediated protein assembly has potential application to many different proteins.

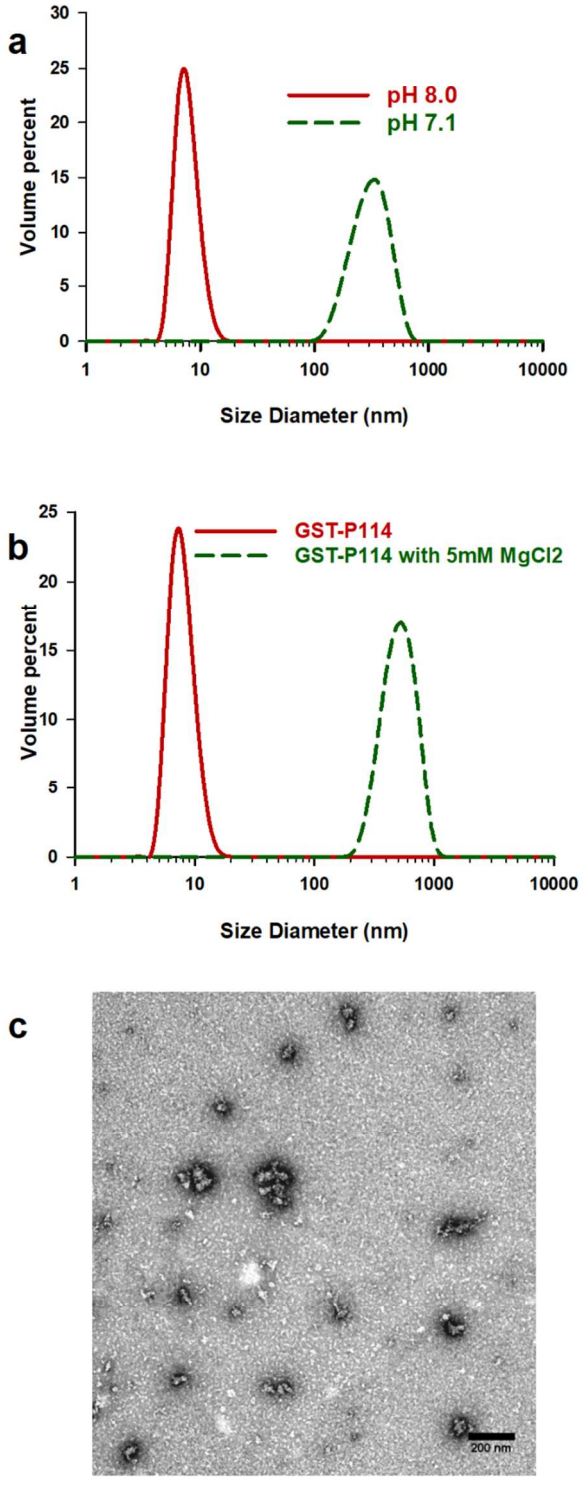

Figure 8. Nanoparticle formation of GST-P_{11}4 at 0.5 mg/mL with pH alteration or addition of Mg^{2+}. (a) GST-P_{11}4 in 50 mM Tris-HCl buffer forms nanoparticles when pH was decreased

from 8.0 to 7.1 (b) Formation of GST-P_{11}4 nanoparticles in 10 mM Tris-HCl buffer pH 8.0 with the addition of 5 mM $MgCl_2$. (c) TEM of GST-P_{11}4 nanoparticles formed in (b).

CONCLUSIONS

In summary, we have demonstrated the controlled formation of protein nanoparticles driven by self-assembly peptide linked to the protein, using pH in buffered solutions or metal-ion Mg^{2+} as two independent modulating parameters. Molecular mechanisms have been proposed to elucidate how peptide-peptide and protein-peptide interactions are regulated by these two key factors, and the intermolecular contact points between protein-peptide monomers involved in nanoparticle formation have been identified by chemical cross-linking mass spectrometry. We have also shown that salt type and ionic strength of the solution influences nanoparticle size and degree of self-assembly. Importantly, pH and $MgCl_2$ concentration can be varied independently or in combination to control nanoparticle size. Self-assembly resulting from combination of these two modulators, provides options to cater for nanoparticle formation based on the functionality of the protein and its intended application.

Strikingly, the formation of protein nanoparticles does not affect the enzyme activity of proteins within the nanoparticles formed under a broad range of assembly conditions. Furthermore, protein nanoparticles are stable to a change in conditions once formed and retain their size over long periods of storage. Nevertheless, formation of nanoparticles is also reversible – they can be disassembled into monomers through desalting of buffer to remove the initiator (*e.g.* Mg^{2+}). This study extends our understanding of the mechanism of salt and pH-mediated protein nanoparticle formation and offers attractive flexibility to select a variety of conditions for on-demand protein self-assembly without compromising protein functionality. The molecular

insights into peptide-driven protein self-assembly can guide the design of future protein nanomaterials whose properties are modulated through changing solution conditions, eliminating the need to change the molecular design or amino acid sequence of the protein-peptide construct. Compared to existing protein nanoparticle technology such as virus-like particles or computationally designed protein nanoparticles, the research presented here offers great flexibility in preparing protein nanoparticles of tunable sizes using one molecular construct. Such flexibility is expected to underpin the broader applications of protein nanoparticles, for example, as biocatalysts and in bio-separations.

MATERIALS AND METHODS

Expression and purification of BCA-P_{11}4, GST-P_{11}4, WT-BCA and WT-tyrosinase. The fusion protein BCA-P_{11}4 was expressed as a single construct in *E. coli* cells and purified as previously described.[9] Briefly, the plasmid pET28a-BCA-P_{11}4 encoding bovine carbonic anhydrase linked to P_{11}4 peptide *via* a GS-linker was transformed into *E.coli* BL21 (DE3) (New England Biolabs Inc.) and cells were grown in terrific broth. Expression of BCA-P_{11}4 was initiated by 1 mM IPTG and culturing continued for 16 h at 20 °C. Cells were lysed and the supernatant collected after centrifugation was purified using immobilized metal-ion affinity chromatography (Profinity IMAC, Biorad laboratories). Stepwise increase of imidazole from 24 to 200 mM in 50 mM Tris-HCl + 0.5 M NaCl pH 8.0 buffer eluted the bound fusion protein. Pure protein fractions were buffer exchanged by a desalting column (G25 Sephadex, GE Healthcare) into either 10 mM Tris-HCl buffer (pH 8.0) for metal-ion screening and full-factorial experiments, or 50 mM Tris-HCl buffer (pH 8.0) for other experiments. Similar conditions of growth, expression and purification were used to produce WT-BCA. GST-P_{11}4 was also

expressed as a single construct using pET28a-GST-$P_{11}4$ plasmid prepared by GenScript (Piscataway, NJ, USA) and *E. coli* BL21 (DE3) as protein production host. Expression and cell lysis procedures were performed similarly to that for BCA-$P_{11}4$. For the purification using IMAC column, GST-$P_{11}4$ was eluted using a gradient of 0-500mM imidazole in 20 mM Tris-HCl pH 8.0 buffer. Desalting of purified GST-$P_{11}4$ into the desired buffer condition was performed as described for BCA-$P_{11}4$. WT-Tyrosinase (UniProt ID– B2ZB02) was produced using *E.coli* BL21 (DE3) cells transformed with pET28a-WT-Tyrosinase plasmid prepared by GenScript (Piscataway, NJ, USA) and grown in terrific broth. Recombinant protein expression was induced with 1 mM IPTG and cells were grown at 20°C overnight. Lysed cell supernatant was purified using IMAC (HisTrap FF, 5mL) and eluted with 200mM imidazole in 50 mM Tris-HCl + 0.5 M NaCl pH 8.0 buffer and desalted into 10 mM Tris-HCl buffer (pH 8.0).

Size measurement using dynamic light scattering. A Zetasizer Nano (Malvern Instruments) was used to monitor formation of nanoparticles. The size of BCA-$P_{11}4$ particles in solution (1 mL) was measured under a range of conditions using the Zetasizer software. Three independent experiments with each comprising 12 cycles were performed to collect data for each experimental condition.

Effects of buffers and temperature on BCA-$P_{11}4$ nanoparticle formation. The effects of four factors namely pH, protein concentration, temperature and metal-ions on formation of BCA-$P_{11}4$ nanoparticle were evaluated. The effect of pH was studied at a fixed protein concentration of 0.5 mg/mL and pH was adjusted using 5 M or 1 M acetic acid for fine adjustment. The effect of varying protein concentration was evaluated at pH 6.8±0.1. Stock solutions of 0.5 M NH_4Cl, $MgCl_2$, NaCl, $NaNO_3$ and Na_2SO_4 were prepared in 10 mM Tris-HCl pH 8.0 and the required volume was added to BCA-$P_{11}4$ sample in 10 mM Tris-HCl pH 8.0 to achieve a final salt

concentration of 50, 100 and 200 mM and protein concentration of 0.5 mg/mL. For evaluation at other pH values, BCA-P_{11}4 with added salts was prepared as above and adjusted to desired pH and the temperature was maintained at 25°C. Exceptions to this were experiments testing temperature dependence where 1 mL BCA-P_{11}4 solution of 0.5 mg/mL in 50 mM Tris-HCl pH 8.0 was incubated at the respective temperatures in a heating block for 5 min before assaying.

Chemical cross-linking of BCA-P_{11}4 nanoparticles and mass spectrometry analysis. The chemical cross-linking reaction of BCA-P_{11}4 self-assembled nanoparticle was performed using either chemical cross-linker EDC/sNHS (Sigma Aldrich) or BS3 (ThermoFisher Scientific) following the methods previously described.[41,42] The self-assembly of BCA-P_{11}4 nanoparticles was initiated in 20 mM potassium phosphate buffer, confirmed by dynamic light scattering (DLS) measurement and the cross-linking reaction was started by mixing freshly prepared cross-linking agents with BCA-P_{11}4 nanoparticles. The cross-linking reaction mixtures each contained 0.5 mg/mL nanoparticles (ca. 0.016 mM protein monomers) with either 10 mM EDC/5 mM sNHS or 10 mM BS3 in 40 µL final volume. The control sample was prepared by adding water instead of chemical cross-linkers into the BCA-P_{11}4 nanoparticles. The cross-linking mixtures were incubated at room temperature for 45 min followed by quenching with 10 µL 500 mM DTT and 10 µL 1 M Tris-HCl pH 7 for EDC/sNHS and BS3, respectively.

The quenched cross-linked protein solutions were then separated by SDS-PAGE (Bolt™ 4-12% Bis-Tris Plus Gels, Invitrogen™) and protein bands stained with Coomassie blue G250. Crosslinked proteins were identified as those that migrated at higher molecular weight and the corresponding SDS-PAGE bands were excised for analysis by mass spectrometry. Briefly, the crosslinked proteins were digested with trypsin and analyzed by nanoLC-ESI-MS/MS. The

crosslinked peptides were identified by software Byonic and P-link 2.0 from the obtained MS data.

Stability of BCA-P_{11}4 nanoparticles over storage. BCA-P_{11}4 nanoparticles formed at pH 6.5 in 50 mM Tris-HCl buffer at 0.5 mg/mL protein concentration was stored in 1.5 mL plastic micro centrifuge tubes at 4 ^{o}C for 30 days, followed by analysis using dynamic light scattering.

Disassembly of protein nanoparticles by removal of magnesium ions. BCA-P_{11}4 at 1.5 mg/mL was triggered to form nanoparticles using 5 mM $MgCl_2$ in 10mM Tris-HCl pH 8.0 buffer. Gel filtration chromatography was performed using 5 mL Hitrap Desalting columns (GE Healthcare) connected to AKTA pure chromatography system (GE Healthcare). The column was equilibrated with 10 mM Tris-HCl buffer pH 8.0 at a flow rate of 1 mL/min and 1 mL of the BCA-P_{11}4 nanoparticle sample was injected into the column using the sample loop, followed by elution using 10 mM Tris-HCl buffer pH 8.0. Protein sample elution was collected from a UV rise of 100 mAU to a UV drop of 100 mAU to ensure protein was completely devoid of magnesium ions. Eluate was analyzed for particle size using dynamic light scattering.

Self-assembly of BCA-P_{11}4 in the presence of other charged biomolecules. The effect of the presence of other charged proteins in solution during BCA-P_{11}4 self-assembly was studied. A 1 mL mixture containing 0.8 mg/mL BCA-P_{11}4 and 0.5 mg/mL WT-BCA was prepared in 10 mM Tris-HCl pH8 buffer. To the mixture $MgCl_2$ was added to a final concentration of 20 mM. Similarly, a 1 mL sample mixture of 0.8 mg/mL BCA-P_{11}4 and 0.5 mg/mL WT-tyrosinase was prepared in 10 mM Tris-HCl pH8 buffer to which 20mM $MgCl_2$ was added. In a separate sample mixture of BCA-P_{11}4 and WT-tyrosinase, the pH was reduced to pH 7.2 using acetic acid prior to addition of 20mM $MgCl_2$. To test the independent effect of pH, the pH of BCA-P_{11}4 and WT-

tyrosinase mixture was reduced from 8.0 to 6.4 using acetic acid. In all cases, the particle size before and after initiating self-assembly was determined using dynamic light scattering method.

Transmission electron microscopy. Negative staining of protein nanoparticles was performed on carbon coated 200 mesh copper grids (GSCu200CC, Proscitech, QLD Australia) by an established protocol[43] using uranyl acetate stain. Details of sample preparation was reported previously.[9] Samples were visualized at 200 kV using FEI, Tecnai G2 T20 TWIN LaB6 transmission electron microscopy.

Two-level full factorial design of nanoparticle assembly. A factorial design experiment using a two-level design was used to model the BCA-P_{11}4 nanoparticle formation. This method examined 4 factors (pH, temperature, $MgCl_2$ concentration and protein concentration) at two levels (Table S3) to determine the major factors and interaction effects on BCA-P_{11}4 nanoparticle formation. A 2^4 full factorial design with 4 center point replicates consisting a total of 20 experiments was performed in randomized order. The particle sizes for each condition was measured by dynamic light scattering and were used as the response variable. The center point values were determined as the average of low and high level values. Response data were analyzed using statistical software Design- Expert 10® (Stat-Ease, Inc. Minneapolis, USA).

Esterase activity of BCA-P_{11}4 using *p*-nitrophenyl acetate (pNPA) assay. The enzyme activities of BCA-P_{11}4 in monomeric and nanoparticle forms were determined using the *p*-nitrophenylacetate (pNPA) assay[44] with minor modifications. Enzyme samples (3 μg protein) were incubated in buffer (50 mM HEPES pH 8.0 containing 50 mM Na_2SO_4) containing 1 mM of pNPA at 25°C with a final volume of 0.2 mL in a 96-well microplate. The product formation was continuously monitored at 405 nm over 10 min by spectrophotometer microplate reader (Infinite 200Pro, Tecan).

ASSOCIATED CONTENT

Supporting Information Available: Details of amino acid sequence of GST-$P_{11}4$, charges of $P_{11}4$, BCA and BCA-$P_{11}4$ at different pH, effects of temperature and protein concentration, two-level full factorial model including design table, residual analysis, ANOVA table and regression model, size of protein nanoparticle at different conditions, cross-linking reaction, SDS-PAGE, mass spectrometry analysis of cross-lined peptides, stability of protein nanoparticles, disassembly of protein particles, and self-assembly in the presence of other molecules are provided (PDF). This material is available free of charge *via* the Internet at http://pubs.acs.org.

The authors declare no competing financial interests.

AUTHOR INFORMATION

Corresponding Author

*Email: lizhong.he@monash.edu (L.H)

ORCID

Lizhong He: 0000-0001-6569-526X

Funding Sources

This project is supported by the Australian Research Council (ARC) through the ARC Research Hub for Energy-efficient Separation (IH170100009). BKS acknowledges the Monash University Institute of Graduate Research (MIGR) and top-up scholarships offered by Monash University and Commonwealth Scientific and Industrial Research Organisation

(CSIRO), respectively. LH acknowledges the Seed Funding from Faculty of Engineering, Monash University.

ACKNOWLEDGMENT

The authors thank Dr David Steer and the Monash Biomedical Proteomics Facility for mass spectrometry analysis. We thank Ms Tayyaba Younas and Monash Centre for Electron Microscopy and The Clive and Ramaciotti Centre for Structural Cryo-Electron Microscopy for TEM sample preparation and imaging. We acknowledge Mr. Rakesh Goud for assistance with statistical analysis.

REFERENCES

(1) Zhang, S. Fabrication of Novel Biomaterials through Molecular Self-Assembly. *Nat. Biotechnol.* **2003**, *21*, 1171–1178.

(2) Kostiainen, M. a; Kasyutich, O.; Cornelissen, J. J. L. M.; Nolte, R. J. M. Self-Assembly and Optically Triggered Disassembly of Hierarchical Dendron-Virus Complexes. *Nat. Chem.* **2010**, *2*, 394–399.

(3) Fan, Z.; Sun, L.; Huang, Y.; Wang, Y.; Zhang, M. Bioinspired Fluorescent Dipeptide Nanoparticles for Targeted Cancer Cell Imaging and Real-Time Monitoring of Drug Release. *Nat. Nanotechnol.* **2016**, *11*, 388–394.

(4) Ku, T. H.; Chien, M. P.; Thompson, M. P.; Sinkovits, R. S.; Olson, N. H.; Baker, T. S.; Gianneschi, N. C. Controlling and Switching the Morphology of Micellar Nanoparticles with Enzymes. *J. Am. Chem. Soc.* **2011**, *133*, 8392–8395.

(5) King, N. P.; Sheffler, W.; Sawaya, M. R.; Vollmar, B. S.; Sumida, J. P.; André, I.; Gonen, T.; Yeates, T. O.; Baker, D. Computational Design of Self-Assembling Protein Nanomaterials with Atomic Level Accuracy. *Science* **2012**, *336*, 1171–1174.

(6) King, N. P.; Bale, J. B.; Sheffler, W.; McNamara, D. E.; Gonen, S.; Gonen, T.; Yeates, T. O.; Baker, D. Accurate Design of Co-Assembling Multi-Component Protein Nanomaterials. *Nature* **2014**, *510*, 103–108.

(7) Hudalla, G. a; Sun, T.; Gasiorowski, J. Z.; Han, H.; Tian, Y. F.; Chong, A. S.; Collier, J. H. Gradated Assembly of Multiple Proteins into Supramolecular Nanomaterials. *Nat. Mater.* **2014**, *13*, 829–836.

(8) Park, W. M.; Champion, J. A. Thermally Triggered Self-Assembly of Folded Proteins into Vesicles. *J. Am. Chem. Soc.* **2014**, *136*, 17906–17909.

(9) Shanbhag, B. K.; Liu, B.; Fu, J.; Haritos, V. S.; He, L. Self-Assembled Enzyme Nanoparticles for Carbon Dioxide Capture. *Nano Lett.* **2016**, *16*, 3379–3384.

(10) Patterson, D. P.; Desai, A. M.; Holl, M. M. B.; Marsh, E. N. G. Evaluation of a Symmetry-Based Strategy for Assembling Protein Complexes. *RSC Adv.* **2011**, *1*, 1004–1012.

(11) James F. Ross, Angela Bridges, Jordan M. Fletcher, Deborah Shoemark, Dominic Alibhai, Harriet E. V. Bray, Joseph L. Beesley, William M. Dawson, Lorna R. Hodgson, Judith Mantell, Paul Verkad, Colin M. Edge, Richard B. Sessions , David Tew, and D. N. W. Decorating Self-Assembled Peptide Cages with Proteins. *ACS Nano* **2017**, *11*, 7901–7914.

(12) Kanekiyo, M.; Wei, C.-J.; Yassine, H. M.; McTamney, P. M.; Boyington, J. C.; Whittle, J.

R. R.; Rao, S. S.; Kong, W.-P.; Wang, L.; Nabel, G. J. Self-Assembling Influenza Nanoparticle Vaccines Elicit Broadly Neutralizing H1N1 Antibodies. *Nature* **2013**, *499*, 102–106.

(13) Shang, L.; Nienhaus, K.; Nienhaus, G. U. Engineered Nanoparticles Interacting with Cells: Size Matters. *J. Nanobiotechnology* **2014**, *12*, 5.

(14) Walkey, C. D.; Olsen, J. B.; Guo, H.; Emili, A.; Chan, W. C. W. Nanoparticle Size and Surface Chemistry Determine Serum Protein Adsorption and Macrophage Uptake. *J. Am. Chem. Soc.* **2012**, *134*, 2139–2147.

(15) Herrera Estrada, L. P.; Champion, J. a. Protein Nanoparticles for Therapeutic Protein Delivery. *Biomater. Sci.* **2015**, *3*, 787–799.

(16) Moses O Oyewumi1, Amit Kumar, Z. C. Nano-Microparticles as Immune Adjuvants: Correlating Particle Sizes and the Resultant Immune. *Expert Rev Vaccines.* **2010**, *9*, 1095–1107.

(17) Aggeli, A.; Bell, M.; Carrick, L. M.; Fishwick, C. W. G.; Harding, R.; Mawer, P. J.; Radford, S. E.; Strong, A. E.; Boden, N. pH as a Trigger of Peptide -Sheet Self-Assembly and Reversible Switching between Nematic and Isotropic Phases. *J. Am. Chem. Soc.* **2003**, *125*, 9619–9628.

(18) Shi, J.; Gao, Y.; Zhang, Y.; Pan, Y.; Xu, B. Calcium Ions to Cross-Link Supramolecular Nanofibers to Tune the Elasticity of Hydrogels over Orders of Magnitude. *Langmuir* **2011**, *27*, 14425–14431.

(19) Kuang, Y.; Gao, Y.; Shi, J.; Lin, H.-C.; Xu, B. Supramolecular Hydrogels Based on the

Epitope of Potassium Ion Channels. *Chem. Commun. (Camb).* **2011**, *47*, 8772–8774.

(20) Hassouneh, W.; Fischer, K.; MacEwan, S. R.; Branscheid, R.; Fu, C. L.; Liu, R.; Schmidt, M.; Chilkoti, A. Unexpected Multivalent Display of Proteins by Temperature Triggered Self-Assembly of Elastin-like Polypeptide Block Copolymers. *Biomacromolecules* **2012**, *13*, 1598–1605.

(21) Wheeldon, I. R.; Gallaway, J. W.; Barton, S. C.; Banta, S. Bioelectrocatalytic Hydrogels from Electron-Conducting Metallopolypeptides Coassembled with Bifunctional Enzymatic Building Blocks. *Proc. Natl. Acad. Sci. U. S. A.* **2008**, *105*, 15275–15280.

(22) Wheeldon, I. R.; Campbell, E.; Banta, S. A Chimeric Fusion Protein Engineered with Disparate Functionalities-Enzymatic Activity and Self-Assembly. *J. Mol. Biol.* **2009**, *392*, 129–142.

(23) McManus, J. J.; Charbonneau, P.; Zaccarelli, E.; Asherie, N. The Physics of Protein Self-Assembly. *Curr. Opin. Colloid Interface Sci.* **2016**, *22*, 73–79.

(24) Kyle, S.; Aggeli, A.; Ingham, E.; McPherson, M. J. Recombinant Self-Assembling Peptides as Biomaterials for Tissue Engineering. *Biomaterials* **2010**, *31*, 9395–9405.

(25) Carrick, L. M.; Aggeli, A.; Boden, N.; Fisher, J.; Ingham, E.; Waigh, T. a. Effect of Ionic Strength on the Self-Assembly, Morphology and Gelation of pH Responsive β-Sheet Tape-Forming Peptides. *Tetrahedron* **2007**, *63*, 7457–7467.

(26) Aggeli, A.; Bell, M.; Carrick, L. M.; Fishwick, C. W. G.; Harding, R.; Mawer, P. J.; Radford, S. E.; Strong, A. E.; Boden, N. pH as a Trigger of Peptide β-Sheet Self-Assembly and Reversible Switching between Nematic and Isotropic Phases. *J. Am. Chem.*

Soc. **2003**, *125*, 9619–9628.

(27) Quan, L.; Wei, D.; Jiang, X.; Liu, Y.; Li, Z.; Li, N.; Li, K.; Liu, F.; Lai, L. Resurveying the Tris Buffer Solution: The Specific Interaction between Tris(hydroxymethyl)aminomethane and Lysozyme. *Anal. Biochem.* **2008**, *378*, 144–150.

(28) Taha, M.; Lee, M.-J. Interactions of TRIS [Tris(hydroxymethyl)aminomethane] and Related Buffers with Peptide Backbone: Thermodynamic Characterization. *Phys. Chem. Chem. Phys.* **2010**, *12*, 12840–12850.

(29) Collins, K. D. Why Continuum Electrostatics Theories Cannot Explain Biological Structure, Polyelectrolytes or Ionic Strength Effects in Ion-Protein Interactions. *Biophys. Chem.* **2012**, *167*, 33–49.

(30) Dougherty, D. a. Cation-Pi Interactions in Chemistry and Biology: A New View of Benzene, Phe, Tyr, and Trp. *Science* **1996**, *271*, 163–168.

(31) Giese, M.; Albrecht, M.; Rissanen, K. Experimental Investigation of Anion-π Interactions - Applications and Biochemical Relevance. *Chem. Commun. (Camb).* **2015**, *52*, 1778–1795.

(32) Watt, M. M.; Zakharov, L. N.; Haley, M. M.; Johnson, D. W. Selective Nitrate Binding in Competitive Hydrogen Bonding Solvents: Do Anion-π Interactions Facilitate Nitrate Selectivity? *Angew. Chemie - Int. Ed.* **2013**, *52*, 10275–10280.

(33) Warden, A. C.; Williams, M.; Peat, T. S.; Seabrook, S. A.; Newman, J.; Dojchinov, G.; Haritos, V. S. Rational Engineering of a Mesohalophilic Carbonic Anhydrase to an Extreme Halotolerant Biocatalyst. *Nat. Commun.* **2015**, *6*, 10278.

(34) Gokarn, Y. R.; Fesinmeyer, R. M.; Saluja, A.; Razinkov, V.; Chase, S. F.; Laue, T. M.; Brems, D. N. Effective Charge Measurements Reveal Selective and Preferential Accumulation of Anions, but Not Cations, at the Protein Surface in Dilute Salt Solutions. *Protein Sci.* **2011**, *20*, 580–587.

(35) Dexter, A. F.; Malcolm, A. S.; Middelberg, A. P. J. Reversible Active Switching of the Mechanical Properties of a Peptide Film at a Fluid-Fluid Interface. *Nat. Mater.* **2006**, *5*, 502–506.

(36) Dooley, K.; Kim, Y. H.; Lu, H. D.; Tu, R.; Banta, S. Engineering of an Environmentally Responsive Beta Roll Peptide for Use as a Calcium-Dependent Cross-Linking Domain for Peptide Hydrogel Formation. *Biomacromolecules* **2012**, *13*, 1758–1764.

(37) Israelachvili, J. Electrostatic Forces Between Surfaces in Liquid. In *Intermolecular and Surface Forces*; Academic Press: Amsterdam, 2011; pp 291–340.

(38) Dai, B.; Kang, S.; Huynh, T.; Lei, H.; Castelli, M.; Hu, J.; Zhang, Y.; Zhou, R. Salts Drive Controllable Multilayered Upright Assembly of Amyloid-like Peptides at Mica / Water Interface. *Proc. Natl. Acad. Sci. U. S. A.* **2013**, *110*, 8543–8548.

(39) Bock, C. W.; Kaufman, a; Glusker, J. P. Coordination of Water to Magnesium Cations. *Inorg. Chem.* **1994**, *33*, 419–427.

(40) Zheng, H.; Chruszcz, M.; Lasota, P.; Lebioda, L. Data Mining of Metal Ion Environments Present in Protein Structures. *J. Inorg. Biochem.* **2008**, *102*, 1765–1776.

(41) Sinz, A.; Wang, K. Mapping Protein Interfaces with a Fluorogenic Cross-Linker and Mass Spectrometry: Application to Nebulin− Calmodulin Complexes. *Biochemistry* **2001**, *40*,

7903–7913.

(42) Schmidt, A.; Kalkhof, S.; Ihling, C.; Cooper, D. M.; Sinz, A. Mapping Protein Interfaces by Chemical Cross-Linking and Fourier Transform Ion Cyclotron Resonance Mass Spectrometry: Application to a Calmodulin / Adenylyl Cyclase 8 Peptide Complex. *Eur J Mass Spectrom (Chichester, Eng)* **2005**, *11*, 525–534.

(43) Booth, D. S.; Avila-Sakar, A.; Cheng, Y. Visualizing Proteins and Macromolecular Complexes by Negative Stain EM: From Grid Preparation to Image Acquisition. *J. Vis. Exp.* **2011**, 58, 3227.

(44) Pocker Y, S. J. The Catalytic Veratility of Erythrocyte Carbonic Anhydrase VII. Kinetic Studies of Esterase Activity and Competitive Inhibition by Substrate Analogs. *Biochemistry* **1968**, *7*, 3021–3031.

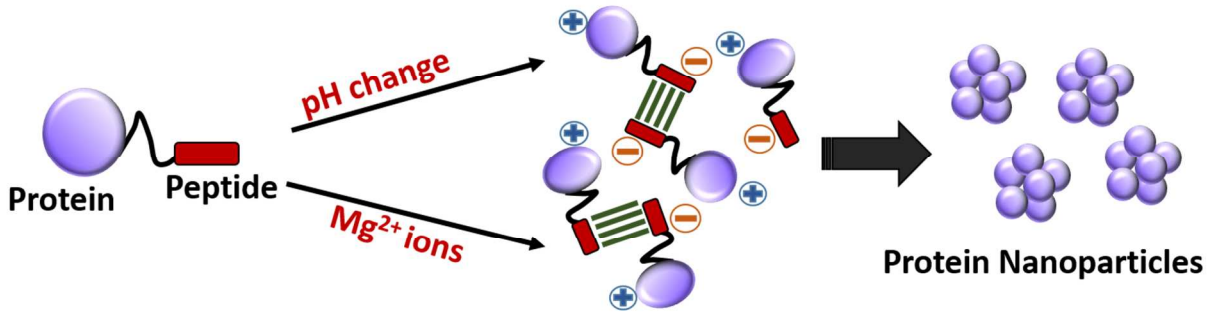

Table of contents graphic